Los Alamos NATIONAL LABORATORY EST.1943

LA-UR-19-32289 (Accepted Manuscript)

Simultaneous Trapping of Electromagnetic Ion Cyclotron and Magnetosonic Waves by Background Plasmas

Yuan, Zhigang
Yu, Xiongdong
Ouyang, Zhihai
Yao, Fei
Huang, Shiyong
Funsten, Herbert O. III

Provided by the author(s) and the Los Alamos National Laboratory (2020-08-19).

To be published in: Journal of Geophysical Research: Space Physics

DOI to publisher's version: 10.1029/2018JA026149

Permalink to record: http://permalink.lanl.gov/object/view?what=info:lanl-repo/lareport/LA-UR-19-32289

Disclaimer:
Los Alamos National Laboratory, an affirmative action/equal opportunity employer, is operated by Triad National Security, LLC for the National Nuclear Security Administration of U.S. Department of Energy under contract 89233218CNA000001. By approving this article, the publisher recognizes that the U.S. Government retains nonexclusive, royalty-free license to publish or reproduce the published form of this contribution, or to allow others to do so, for U.S. Government purposes. Los Alamos National Laboratory requests that the publisher identify this article as work performed under the auspices of the U.S. Department of Energy. Los Alamos National Laboratory strongly supports academic freedom and a researcher's right to publish; as an institution, however, the Laboratory does not endorse the viewpoint of a publication or guarantee its technical correctness.

RESEARCH LIBRARY

Check for updates

Accepted Article

Yuan Z.G. (Orcid ID: 0000-0002-3756-3507)

Yu Xiongdong (Orcid ID: 0000-0002-1179-1667)

Huang Shiyong (Orcid ID: 0000-0002-3595-2525)

Funsten Herbert, O. (Orcid ID: 0000-0002-6817-1039)

Simultaneous trapping of EMIC and MS waves by background plasmas

Zhigang Yuan[1]*, Xiongdong Yu[1], Zhihai Ouyang[1], Fei Yao[1], and Shiyong Huang[1], H. O. Funsten[2]

[1]School of Electronic Information, Wuhan University, Wuhan, China

[2]ISR Division, Los Alamos National Laboratory, Los Alamos, New Mexico 87545, USA

*Correspondence to: Zhigang Yuan

Communication message:

Dr. Zhigang Yuan

School of Electronic Information

Wuhan University

Wuhan 430072, P. R. China

E-MAIL: y_zgang@vip.163.com

Tel: +86-027-68754720

This article has been accepted for publication and undergone full peer review but has not been through the copyediting, typesetting, pagination and proofreading process which may lead to differences between this version and the Version of Record. Please cite this article as doi: 10.1029/2018JA026149

© 2019 American Geophysical Union. All rights reserved.

Abstract: Electromagnetic ion cyclotron waves and fast magnetosonic waves are found to be simultaneously modulated by background plasma density: both kinds of waves were observed in high plasma density regions but vanished in low density regions. Theoretical analysis based on Snell's law and linear growth theory have been utilized to investigate the physical mechanisms driving such modulation. It is suggested that the modulation of fast magnetosonic waves might be due to trapping by plasma density structures, which results from a conservation of the parameter Q during their propagation. Here $Q = nr\sin\psi$, with n the refractive index, r the radial distance, and ψ the wave azimuthal angle. As for electromagnetic ion cyclotron waves, the modulation might be owed to the ion composition difference between different plasma density regions. Our results indicate the alternative mechanism for simultaneous appearance of electromagnetic ion cyclotron waves and fast magnetosonic waves (rather than wave excitations of both two wave emissions), which might take combined effects on the evolution of radiation belt electrons.

Key words: EMIC waves; MS waves; Wave trapping; Ring current ions; Van Allen Probe.

Introduction

In the inner magnetosphere, there exist two kinds of electromagnetic emissions which excitations are relevant to ring current ions: electromagnetic ion cyclotron (EMIC) waves and fast magnetosonic (MS) waves. Generally, EMIC waves are electromagnetic emissions with frequencies below ion cyclotron frequencies, and they are often divided into three distinct bands: Hydrogen band (H^+ band), Helium band (He^+ band), and Oxygen band (O^+ band)

© 2019 American Geophysical Union. All rights reserved.

Accepted Article

(*Anderson et al.*, 1992; *Min et al.*, 2012; *Wang et al.*, 2015; *Yu et al.*, 2015). H^+ band EMIC waves have frequencies below gyrofrequencies of protons (H^+) but above gyrofrequencies of helium ions (He^+), and He^+ band EMIC waves have frequencies below gyrofrequencies of He^+ but above gyrofrequencies of oxygen ions (O^+), while frequencies of O^+ band EMIC waves are below gyrofrequencies of oxygen ions (O^+). It has been demonstrated that EMIC waves are excited by unstable ring current ion distributions, such as temperature anisotropic distributions (*Kennel and Petschek*, 1966; *Lee et al.*, 2017), loss-cone like distributions (*Denton et al.*, 1992), ring distributions (*Yu et al.*, 2016, 2018), etc. It is widely thought that H^+ band and He^+ band EMIC waves are excited near the equator with small wave normal angles and left-hand polarizations, which might become more oblique as they propagate away from their source regions (*Rauch and Roux*, 1982). The occurrence rates of the H^+ band and He^+ band EMIC waves depend upon the orientation of the IMF (*Nakamura et al.*, 2016; *Park et al.*, 2017). The high occurrence region for the H_+ band moves from the dawnside to the dayside region when the IMF changes from northward IMF to southward IMF. But for the He^+ band, the high occurrence region is shifted into the lower L-shell ($L < 8$) in the dusk sector. In recent several decades, EMIC waves have obtained more and more focus. One of the most important reasons is due to their capabilities of making important contributions to the evolution of magnetospheric particles (*Yuan et al.*, 2010, 2012, 2013, 2014; *Zhang et al.*, 2010), especially for rapid loss of radiation belts (*Summers*, 2005; *Wang et al.*, 2014; *Usanova et al.*, 2014).

On the other hand, MS waves, named also as equatorial noise (*Russell et al.*, 1970), have been demonstrated to be resulted from the ion Bernstein instability driven by energetic ions

© 2019 American Geophysical Union. All rights reserved.

Accepted Article

with ring velocity distributions ($\partial f/\partial v_{\perp} > 0$) (e.g. *Balikhin et al.*, 2015). These waves often have frequencies between the proton cyclotron frequencies (f_{cH}) and lower hybrid resonant frequencies (f_{LH}), and propagate (quasi-)perpendicularly with respect to the background magnetic field (*Meredith et al.*, 2008; *Ma et al.*, 2013). Recent studies have demonstrated that dense background plasma densities can restrain the growth rates and lower frequency bands of MS waves as excited in source regions (*Yuan et al.*, 2017; *Yuan, Ouyang et al.*, 2018). Results of ray tracing indicate that MS waves can propagate not only along the radial direction, but also in the azimuthal direction (*Xiao et al.*, 2012). It has been demonstrated that MS waves can not only accelerate radiation belt electrons (*Horne et al.*, 2007; *Ma et al.*, 2016), but also heat thermal electrons and ions (*Sun et al.*, 2017; *Yuan, Yu et al.*, 2018). Especially, MS waves have been reported to play an important role in the formation of butterfly pitch angle distributions of radiation belt electrons (e.g. *Xiao et al.*, 2015).

Although the free energy supporting the growth of both EMIC waves and MS waves are usually provided by ring current protons, only few MS waves are observed accompanied with EMIC waves, which might be due to the low temperature anisotropy of proton ring distributions (*Min et al.*, 2016). In this paper, we report a typical event observed by the Van Allen Probe B on 9 October 2013, where EMIC waves and MS waves occurred simultaneously in high plasma density regions but vanished in low density regions. That is, EMIC waves and MS waves are modulated by the background plasma density. In virtue of Snell's law and linear growth theory, we show that such a modulation might be resulted from the simultaneous trapping of EMIC waves and MS waves by background plasmas.

Accepted Article

© 2019 American Geophysical Union. All rights reserved.

Observations

In our cases, observation data for magnetic spectrum of MS waves is provided by the Electric and Magnetic Field Instrument Suite and Integrated Science Waves instrument (*Kletzing et al.*, 2013) onboard the Van Allen Probe B, while high-resolution (64 samples/s) magnetic field vectors are analyzed to obtain the dynamic spectrum of EMIC waves (*Yu et al.*, 2018). Flux data attained from the Helium, Oxygen, Proton, and Electron Mass Spectrometer (*Funsten et al.*, 2013) is utilized to derive the proton distributions, which would be used to calculate the linear growth rate. Additionally, the plasma density is attained from the upper hybrid resonant frequencies (*Kurth et al.* 2015).

Figure 1 shows an overview of simultaneously trapping event of EMIC and MS waves. It is shown that during October 8−11 in 2013, a geomagnetic storm, accompanied with enhancements of solar wind dynamic pressures (panel b) and substorms (panel c), entered the main phase after the Bz component of the interplanetary magnetic field (IMF) became southward (panel a). At 0042UT in 9 October 2013, the SYM-H index reached the minimum of -77 nT (panel d), implying a moderate geomagnetic storm. In the recovery phase of this geomagnetic storm, Van Allen Probe B observed both EMIC and MS waves during 0050 UT to 0145UT in 9 October 2013, which are displayed in panels (d-k) in more detail: Figure 1(e) shows the plasma density (N_e), while the magnetic power spectral density (PSD), ellipticity (ε) and wave normal angles (WNA) of MS waves are exhibited in Figure 1(f)−(h), respectively. Additionally, Figure 1(i)−(k) display the magnetic power spectral density (PSD), ellipticity (ε) and wave normal angles (WNA) of EMIC waves, respectively. It is clearly shown in Figure 1(e)−(h) that during this interval, MS waves, with frequencies just below f_{LH}, linear

© 2019 American Geophysical Union. All rights reserved.

Accepted Article

polarization ($\varepsilon \sim 0$) and large wave normal angles (WNA ~ 90°), occurred only in those regions with $N_e > 250$ cm^{-3}. In the meanwhile, He^+ band EMIC waves with frequencies between 0.22 f_{cH} and 0.10f_{cH} are observed with mostly left-hand polarization ($\varepsilon < 0$) and small wave normal angles (WNA < 30°). Again, these EMIC waves are also found only in high density regions ($N_e > 250$ cm^{-3}). That is to say, both EMIC waves and MS waves have been observed to be modulated by the background plasma.

To study this modulation, we have checked the observed velocity distribution data of H^+, He^+, and O^+ and shown in Figure 2(a-c). Ring current protons with energies greater than 2 keV, which are generally the source of free energy supporting growth of EMIC and MS waves, have not significant changes, especially before about 0135 UT (panel a). However, during 0114 UT to 0134 UT, fluxes of protons with energies between 10 eV and 2 keV increased by several orders of magnitude as the satellite moved from high density regions to low density regions, indicating different properties between plasmas in high density regions and in low density regions. In Figure 2(d), the perpendicular components of proton distributions ($f_\perp$) derived from the observed fluxes during 0114 UT to 0134 UT have been illustrated as grey curves. Typically, bold blue (red) curve denotes proton distributions observed at about 0120 (0123) UT in a low–density (high–density) region. Obviously, proton distributions with energies of 10 eV to 2 keV observed in high- and low- density regions are well separated.

It has been demonstrated that the excitation of MS waves could be modulated by the background plasma density so that MS waves occurred only in low density regions (*Yuan et al.*, 2017). In the case reported here, on the contrary, MS waves are observed only in high density regions. As shown in Figure 2(a), there are not significant proton rings detected at

© 2019 American Geophysical Union. All rights reserved.

Accepted Article

energies greater than 2 keV, indicating no free energy for growth of MS waves. Thus, it seems hardly to interpret the modulation of MS waves in this paper from the aspect of excitation source, as demonstrated in *Yuan et al.* (2017). We have also calculated the growth rates of MS waves for our cases, and no significant wave growth are found for MS waves (not shown). In fact, when MS waves propagate nearly in an axis-symmetrical medium, according to Snell's law, the parameter Q = $nr\sin\psi$ is conserved along the ray path (*Chen and Thorne 2012*), where n is the refractive index, r is the radial distance, and ψ is the wave azimuthal angle. As a result, MS waves in the inner magnetosphere would be trapped in some radial plasma density regions, which can be attained by checking the reflection condition Q (ψ = 90°) = nL (*Chen and Thorne*, 2012; *Ma et al.*, 2014). That is to say, these trapped MS waves would be constraint in narrow L-shell but can propagate azimuthally, which might be due to the density gradient (*Kasahara et al.*, 1994).

In order to investigate the trapping of MS waves, we have calculated corresponding Q with in–situ observations of background plasma densities (shown in Figure 3a) and magnetic field magnitudes (shown in Figure 3b). In our calculation, the refractive index of MS waves is simplified under cold plasma approximation as: $n^2 = RL/S$, where R, L, and S are Stix coefficients (*Stix*, 1992). Here only the corresponding Q for MS waves with frequencies of 30 Hz have been calculated and displayed in Figure 2(c). For brevity and clarity, the calculated Q have been normalized to its maximum value Q_{max} during the time interval of interest. It is clearly shown in Figure 2(c) that the calculated Q have been separated into four trapping regions by three troughs which are mainly resulted from the low background plasma densities. Comparing the calculated Q with the observed MS waves (Figure 3d) and N_e (Figure 3a), we

© 2019 American Geophysical Union. All rights reserved.

Accepted Article

can conclude that the modulation of MS waves in our case might be due to wave trapping effects of background plasma density structures.

Discussion

As for EMIC waves, we have calculated the linear growth rate to check whether these observed EMIC waves are modulated by background plasma densities through wave excitations. The proton distributions observed at about 0120 UT and 0123 UT are firstly fitted by multicomponent Maxwellian distributions, which results are shown in Figure 4(a) and (b), respectively. The fitted parameters are shown in Table 1 and 2, respectively. To calculate the linear growth rate, the observed background plasma density and magnetic field are used while cold electrons, protons, helium ions, and oxygen ions of the background plasma are assumed to have Maxwellian distributions with a temperature of 2 eV, 0.6 eV, 0.6 eV, and 1 eV, respectively. Additionally, since the background plasma density was observed to be so dense, dispersion relation and growth rates are solved under cold plasma approximation (*Kennel* 1966; *Chen et al.*, 2010; *Yu et al.*, 2016). Cold plasma dispersion relations with two different ion compositions (H^+:He^+:O^+ = 88:10:02 and 65:10:25) are shown in Figure 4(c)–(d), respectively. Note that since these wave events are observed in the recovery phase of a magnetic storm (cf. Figure 1), in which case the number densities of O^+ can reach about 50% (*Takahashi et al.*, 2008), several cases of high heavy ion compositions are considered. As shown in each dispersion relation panel, three distinct band EMIC wave modes are displayed as well as the whistler wave branch, with the former denoted as solid curves while the latter as dot–dash curves. In the meanwhile, purple points denote the cross-over frequencies (ω_{cr1}

© 2019 American Geophysical Union. All rights reserved.

Accepted Article

and ω_{cr2}) where the whistler branch intersect with EMIC wave modes, while the black horizontal lines denote the cut-off frequencies (ω_{co1} and ω_{co2}). Note that the blue circles in Figure 4(c) indicate the frequency interval of the observed EMIC waves. Since only intense He^+ band EMIC waves are observed, we will focus on the modulation of He^+ band EMIC wave by the background plasma.

Using proton distributions observed at about 0123 UT and 0120 UT (Figure 3a–b), we have calculated the linear growth rate of He^+ band EMIC waves and displayed as solid black curve in Figure 4(e) and solid red curve in Figure 4(f), respectively. To study the influence of the background plasma density, growth rates of He^+ band EMIC waves for other three plasma densities (N_e = 350, 220, and 150 cm^{-3}) are calculated and shown as dashed blue, green, and red curves in Figure 4(e), respectively. As shown in Figure 4(e), for N_e = 550 cm^{-3}, positive growth rates of He^+ band EMIC waves occur in frequencies during 0.08 f_{cH} and 0.22 f_{cH}, which includes the frequency band of the observed EMIC waves (cf. Figure 1i and Figure 4c). It is indicated that these observed EMIC waves can be locally excited. However, as N_e decreases gradually, growth rates of He^+ band EMIC waves are found to increase on the whole, which suggests that density variations might not be the key factor to the modulation of EMIC waves. Additionally, comparison between the dashed red curve in Figure 3e and the solid red curve in Figure 4f (which two have the same plasma densities) suggests that those thermal protons with energies below ~ 2 keV might just make little contribution to the modulation of EMIC waves.

In fact, EMIC waves in the magnetosphere have two different propagation modes: guided mode and unguided mode (*Rauch and Roux*, 1982; *Horne and Thorne*, 1993). For He^+ band

© 2019 American Geophysical Union. All rights reserved.

Accepted Article

EMIC waves, emissions with frequencies between cross-over frequency ω_{cr2} and He^+ gyrofrequency Ω_{He+} are propagating in a guided mode, while those with frequencies between cut-off frequency ω_{co2} and cross-over frequency ω_{cr2} in an unguided mode. To interpret in details, refractive index surfaces for He^+ band EMIC waves are displayed in Figure 5, where guided EMIC waves are denoted as solid black curves while unguided EMIC waves are denoted as dashed colored curves. Note that wave group velocities (v_g) are normal to the corresponding refractive index surfaces. As clearly shown in Figure 5, guided EMIC waves have group velocities (quasi-)parallel with respect to the background magnetic field (B_0) for arbitrary wave normal angle between 0° to 90°, so that they would propagate nearly along with the magnetic field lines, that is, guided EMIC waves would be trapped nearly in a magnetic flux tube. However, group velocities of unguided EMIC waves would become normal to the background magnetic field gradually as wave normal angles increase from 0° to 90°. Thus, when EMIC waves, which are often excited near the equator, propagate away from the equator, guided EMIC waves will return back closely to the same L shells after reflected at points where He^+–O^+ bi–ion frequencies are great than wave frequencies, while unguided EMIC waves will move to large L shells and might be rapidly fade away due to electron Landau damping (*Horne and Thorne,* 1993).

As shown in Figure 4(c) and (e), EMIC waves are observed in the frequency interval between 0.10 f_{cH} and 0.22 f_{cH}, but the calculated growth rates indicate that EMIC waves can be excited locally during 0.08 f_{cH} and 0.22 f_{cH}. Note that here ω_{cr2} = 0.1047 Ω_{cH}. The reason might be that EMIC waves were actually excited with frequencies between 0.10 f_{cH} and 022 f_{cH}, but unguided EMIC waves (0.08 $f_{cH} < \omega < \omega_{cr2}$) have propagated to large L shells so that only

© 2019 American Geophysical Union. All rights reserved.

Accepted Article

those in guided modes ($\omega_{cr2} < \omega < 0.22\ f_{cH}$) could be observed by the satellite. On the other hand, since during the late recovery phase of magnetic storms, oxygen ions could become richer, especially in the low density trough (e.g. *Takahashi et al.*, 2008; *Nosé et al.*, 2015), we have calculated the growth rate of He^+ band EMIC waves in plasmas with other three different ion compositions (H^+:He^+:O^+ = 80:10:20, 75:10:25, and 65:10:25) and the result is illustrated in Figure 4(f) as dashed yellow, green, and blue curves, respectively. It is shown that higher compositions of heavy ions in background plasma would result in a larger ω_{cr2} (denoted as purple circles) and thus a narrower frequency band of positive growth rates (cf. Figure 4f). Especially, when ion compositions become H^+:He^+:O^+ = 65:10:25, ω_{cr2} increases to about 0.2106 Ω_{cH}, in which case EMIC waves have such narrow frequency band (0.01 f_{cH}) as well as small growth rates that they are easily be damped. As a result, EMIC waves can hardly be observed in these regions with richer heavy ion compositions. It is suggested that the modulation of EMIC waves might be own to that richer heavy ion compositions in low density regions suppress the frequency band and growth rate of guided EMIC waves.

Conclusion

In this paper, we have reported a typical case where EMIC waves and MS waves are modulated by background plasma. Using Snell's law and linear growth theory, we have shown that the modulation of MS waves might be due to the trapping effects of the background plasma density. On the other hand, the role of plasma densities, thermal protons, and ion compositions playing in the modulation of EMIC waves are investigated. Our results

© 2019 American Geophysical Union. All rights reserved.

Accepted Article

suggest that the modulation of EMIC waves might be resulted from their different propagation characteristics in regions with different ion compositions. In fact, similar density irregularities have been observed in the dusk sector in the plasmasphere or on the plasmaspheric boundary layers (*Darrouzet et al.*, 2004; *Décréau et al.*, 2005), especially on the plasmapause crossing (*Moldwin et al.*, 2002). Our result suggests that such density structures would be favorable for simultaneous trapping of EMIC and MS waves. Since simultaneously trapped in confined regions, EMIC waves and MS waves might make combined effects on the evolution of magnetospheric particles, especially for radiation belt electrons, which will be studied in the future work.

Acknowledgements

We acknowledge the Van Allen Probes data from the EMFISIS and HOPE instrument obtained from http://emfisis.physics.uiowa.edu/data/index, and http://www.rbsp-ect.lanl.gov/data_pub/, respectively. We thank Craig A. Kletzing for providing the data of the EMFISIS and advice on their usage. The Solar dynamic pressure, AE index and SYM-H index data is provided by SPDF OMNI web at http://omniweb.gsfc.nasa.gov/. This work is supported by the National Natural Science Foundation of China (41874194, 41521063, 41374168) and the National Postdoctoral Programme for Innovative Talents (BX20180222).

Accepted Article

© 2019 American Geophysical Union. All rights reserved.

Reference

Anderson, B. J., R. E. Erlandson, and L. J. Zanetti (1992), A statistical study of Pc1–2 magnetic pulsations in the equatorial magnetosphere: 2. Wave properties, J. Geophys. Res., 97(A3), 3089–3101, doi:10.1029/ 91JA02697.

Balikhin, M. A., Shprits, Y. Y., Walker, S. N., Chen, L., Cornilleau-Wehrlin, N., Dandouras, I., … Weiss, B. (2015). Observations of discrete harmonics emerging from equatorial noise. Nature Communications, 6, 7703.

Chen, L., R. M. Thorne, V. K. Jordanova, C.-P. Wang, M. Gkioulidou, L. Lyons, and R. B. Horne (2010), Global simulation of EMIC wave excitation during the 21 April 2001 storm from coupled RCM-RAM-HOTRAY modeling, J. Geophys. Res., 115, A07209, doi:10.1029/2009JA015075.

Chen, L., and R. M. Thorne (2012), Perpendicular propagation of magnetosonic waves, Geophys. Res. Lett., 39, L14102, doi:10.1029/ 2012GL052485.

Darrouzet, F., Décréau, P. M. E., De Keyser, J., Masson, A., Gallagher, D. L., Santolik, O., Sandel, B. R., Trotignon, J. G., Rauch, J. L., Le Guirriec, E., Canu, P., Sedgemore, F., André, M., and Lemaire, J. F. (2004), Density structures inside the plasmasphere: Cluster observations, *Ann. Geophys.*, 22, 2577-2585, doi:10.5194/angeo-22-2577-2004.

Denton, R. E., M. K. Hudson, and I. Roth (1992), Loss‐cone‐driven ion cyclotron waves in the magnetosphere, *J. Geophys. Res.*, *97*(A8), 12093–12103, doi: 10.1029/92JA00954.

Décréau, P. M. E., Le Guirriec, E., Rauch, J. L., Trotignon, J. G., Canu, P., Darrouzet, F., Lemaire, J., Masson, A., Sedgemore, F., and André, M.(2005), Density irregularities in the plasmasphere boundary player: Cluster observations in the dusk sector, *Adv. Space*

© 2019 American Geophysical Union. All rights reserved.

Accepted Article

Res., 36, 1964–1969.

Funsten, H. O., Skoug, R. M., Guthrie, A. A., MacDonald, E. A., Baldonado, J. R., Harper, R. W., et al. (2013). Helium, oxygen, proton, and electron (HOPE) mass spectrometer for the radiation belt storm probes mission. Space Science Reviews, 179(1-4), 423–484. https://doi.org/10.1007/ s11214-013-9968-7.

Horne, R. B., and R. Thorne (1993), On the preferred source location for the convective amplification of ion cyclotron waves, J. Geophys. Res., 98(A6), 9233–9247.

Horne, R. B., R. M. Thorne, S. A. Glauert, N. P. Meredith, D. Pokhotelov, and O. Santolík (2007), Electron acceleration in the Van Allen radiation belts by fast magnetosonic waves, Geophys. Res. Lett., 34, S09S03, doi:10.1029/L17107.

Kasahara, Y., H. Kenmochi, and I. Kimura (1994), Propagation characteristics of the ELF emissions observed by the satellite Akebono in the magnetic equatorial region, Radio Sci., 29(4), 751–767, doi: 10.1029/94RS00445.

Kletzing, C. A., Kurth, W. S., Acuna, M., MacDowall, R. J., Torbert, R. B., Averkamp, T., et al. (2013). The Electric and Magnetic Field Instrument Suite and Integrated Science (EMFISIS) on RBSP. Space Science Reviews, 179(1-4), 127–181.

Kennel, C. (1966), Low-frequency whistler mode, Phys. Fluids, 9, 2190–2202.

Kennel, C., and H. Petschek (1966), Limit on stably trapped particle fluxes, J. Geophys. Res., 71, 1–28, doi:10.1029/JZ071i001p00001.

Kurth, W. S., De Pascuale, S., Faden, J. B., Kletzing, C. A., Hospodarsky, G. B., Thaller, S., & Wygant, J. R. (2015). Electron densities inferred from plasma wave spectra obtained by the Waves instrument on Van Allen Probes. Journal of Geophysical Research: Space

© 2019 American Geophysical Union. All rights reserved.

Accepted Article

Physics, 120, 904–914.

Lee, D.-Y., Noh, S.-J., Choi, C.-R., Lee, J. J., & Hwang, J. A. (2017). Effect of hot anisotropic He+ ions on the growth and damping of electromagnetic ion cyclotron waves in the inner magnetosphere. Journal of Geophysical Research: Space Physics, 122, 4935–4942. https:// doi.org/10.1002/2016JA023826.

Ma, Q., W. Li, R. M. Thorne, and V. Angelopoulos (2013), Global distribution of equatorial magnetosonic waves observed by THEMIS, Geophys. Res. Lett., 40, 1895–1901, doi:10.1002/grl.50434.

Ma, Q., W. Li, L. Chen, R. M. Thorne, C. A. Kletzing, W. S. Kurth, G. B. Hospodarsky, G. D. Reeves, M. G. Henderson, and H. E. Spence (2014), The trapping of equatorial magnetosonic waves in the Earth's outer plasmasphere, Geophys. Res. Lett., 41, 6307–6313, doi:10.1002/2014GL061414.

Ma, Q. L., Li, W., Thorne, R. M., Bortnik, J., Kletzing, C. A., Kurth, W. S., & Hospodarsky, G. B. (2016). Electron scattering by magnetosonic waves in the inner magnetosphere. Journal of Geophysical Research: Space Physics, 121, 274–285. https://doi.org/10.1002/2015JA021992.

Meredith, N., R. B. Horne, and R. R. Anderson (2008), Survey of magnetosonic waves and proton ring distributions in the Earth's inner magnetosphere, J. Geophys. Res., 113, A06213, doi:10.1029/2007JA012975.

Min, K., J. Lee, K. Keika, and W. Li (2012), Global distribution of EMIC waves derived from THEMIS observations, J. Geophys. Res., 117, A05219, doi:10.1029/2012JA017515.

Min, K., K. Liu, and S. P. Gary (2016), Scalings of Alfvén-cyclotron and ion Bernstein

© 2019 American Geophysical Union. All rights reserved.

Accepted Article

instabilities on temperature anisotropy of a ring‐like velocity distribution in the inner magnetosphere, J. Geophys. Res. Space Physics, 121, 2185–2193, doi: 10.1002/2015JA022134.

Moldwin, M. B., L. Downward, H. K. Rassoul, R. Amin, and R. R. Anderson (2002), A new model of the location of the plasmapause: CRRES results, J. Geophys. Res., 107(A11), 1339, doi:10.1029/2001JA009211.

Nakamura, S., Omura, Y., & Angelopoulos, V. (2016). A statistical study of EMIC rising and falling tone emissions observed by THEMIS. Journal of Geophysical Research: Space Physics, 121, 8374-8391. doi:10.1002/2016JA022353.

Nosé, M., et al. (2015), Formation of the oxygen torus in the inner magnetosphere: Van Allen Probes observations, J. Geophys. Res. Space Physics, 120, 1182–1196, doi:10.1002/2014JA020593.

Park, J.-S., Shue, J.-H., & Kim, K.-H. (2017). Dependence of electromagnetic ion cyclotron wave occurrence on north-south orientation of interplanetary magnetic field: THEMIS observations. Journal of Geophysical Research: Space Physics, 122, 11,354-11,372. https://doi.org/10.1002/2017JA024507

Rauch, J. L., and A. Roux (1982), Ray tracing of ULF waves in a multicomponent magnetospheric plasma: Consequences for the generation mechanism of ion cyclotron waves, J. Geophys. Res., 87, 8191–8198.

Russell, C. T., Holzer, R. E., & Smith, E. J. (1970). OGO 3 observations of ELF noise in the magnetosphere. 2. The nature of the equatorial noise. Journal of Geophysical Research, 75(4), 755–768.

© 2019 American Geophysical Union. All rights reserved.

Accepted article

Stix, T. H. (1992), Waves in Plasmas, Am. Inst. of Phys., New York.

Summers, D. (2005), Quasi-linear diffusion coefficients for field-aligned electromagnetic waves with applications to the magnetosphere, J. Geophys. Res., 110, A08213, doi:10.1029/2005JA011159.

Sun, J. C., Gao, X. L., Lu, Q. M., Chen, L. J., Liu, X., Wang, X. Y., et al. (2017). Spectral properties and associated plasma energization by magnetosonic waves in the Earth's magnetosphere: Particle-in-cell simulations. Journal of Geophysical Research: Space Physics, 122, 5377–5390.

Takahashi, K., S. Ohtani, R. E. Denton, W. J. Hughes, and R. R. Anderson (2008), Ion composition in the plasma trough and plasma plume derived from a Combined Release and Radiation Effects Satellite magnetoseismic study, J. Geophys. Res., 113, A12203, doi:10.1029/2008JA013248.

Usanova, M. E., et al. (2014), Effect of EMIC waves on relativistic and ultrarelativistic electron populations: Ground-based and Van Allen Probes observations, Geophys. Res. Lett., 41, 1375–1381, doi:10.1002/2013GL059024.

Wang, Z., Z. Yuan, M. Li, D. Wang, H. Li, S. Huang, and Z. Qiao (2014), Statistical characteristics of EMIC wave-driven relativistic electron precipitation with observations of POES satellites: Revisit, J. Geophys. Res. Space Physics, 119, 5509–5519, doi:10.1002/2014JA020082.

Wang, D., et al. (2015), Statistical characteristics of EMIC waves: Van Allen Probe observations, J. Geophys. Res. Space Physics, 120, doi:10.1002/ 2015JA021089.

Xiao, F., Q. Zhou, Z. He, and L. Tang (2012), Three-dimensional ray tracing of fast

© 2019 American Geophysical Union. All rights reserved.

Accepted Article

magnetosonic waves, J. Geophys. Res., 117, A06208, doi:10.1029/2012JA017589.

Xiao, F. L., Yang, C., Su, Z. P., Zhou, Q. H., He, Z. G., He, Y. H., et al. (2015). Wave-driven butterfly distribution of Van Allen belt relativistic electrons. Nature Communications, 6(1), 8590. https://doi.org/10.1038/ncomms9590.

Yu, X., Z. Yuan, D. Wang, H. Li, S. Huang, Z. Wang, Q. Zheng,M. Zhou, C. A. Kletzing, and J. R. Wygant (2015), In situ observations of EMIC waves in O^+ band by the Van Allen Probe A, Geophys. Res. Lett., 42, 1312–1317, doi:10.1002/ 2015GL063250.

Yu, X., Z. Yuan, D. Wang, S. Huang, Z. Qiao, T. Yu, and F. Yao (2016), Excitation of oblique O+ band EMIC waves in the inner magnetosphere driven by hot H^+ with ring velocity distributions, J. Geophys. Res. Space Physics, 121, 11,101–11,112, doi:10.1002/2016JA023221.

Yu, X., Yuan, Z., Huang, S., Yao, F., Wang, D., Funsten, H. O., & Wygant, J. R. (2018). Excitation of O^+ band EMIC waves through H^+ ring velocity distributions: Van Allen Probe observations. Geophysical Research Letters, 45, 1271–1276. https://doi.org/10.1002/ 2018GL077109

Yuan, Z., Deng, X., Lin, X., Pang, Y., Zhou, M., Décréau, P. M. E., et al. (2010). Link between EMIC waves in a plasmaspheric plume and a detached sub-auroral proton arc with observations of Cluster and IMAGE satellites. Geophysical Research Letters, 37, L07108. https://doi. org/10.1029/2010GL042711

Yuan, Z., Xiong, Y., Pang, Y., Deng, X., Trotignon, J. G., Lucek, E., & Wang, J. (2012). Wave-particle interaction in a plasmaspheric plume observed by a Cluster satellite. Journal of Geophysical Research, 117, A03205. https://doi.org/10.1029/2011JA017152

© 2019 American Geophysical Union. All rights reserved.

Accepted Article

Yuan, Z., Li, M., Xiong, Y., Li, H., Zhou, M., Wang, D., et al. (2013). Simultaneous observations of precipitating radiation belt electrons and ring current ions associated with the plasmaspheric plume. Journal of Geophysical Research: Space Physics, 118, 4391–4399. https://doi.org/ 10.1002/jgra.50432

Yuan, Z., Xiong, Y., Huang, S., Deng, X., Pang, Y., Zhou, M., et al. (2014). Cold electron heating by EMIC waves in the plasmaspheric plume with observations of the Cluster satellite. Geophysical Research Letters, 41, 1830–1837.

Yuan, Z., X. Yu, S. Huang, D. Wang, and H. O. Funsten (2017), In situ observations of magnetosonic waves modulated by background plasma density, Geophys. Res. Lett., 44, 7628–7633, doi:10.1002/ 2017GL074681.

Yuan, Z., Yu, X., Huang, S., Qiao, Z., Yao, F., & Funsten, H. O. (2018). Cold ion heating by magnetosonic waves in a density cavity of the plasmasphere. Journal of Geophysical Research: Space Physics, 123, 1242–1250.

Yuan, Z., Ouyang, Z., Yu, X., Huang, S., Yao, F., & Funsten, H. O. (2018). Global distribution of proton rings and associated magnetosonic wave instability in the inner magnetosphere. Geophysical Research Letters, 45, 10,160–10,166. https://doi.org/10.1029/ 2018GL079999

Zhang, J.-C., Kistler, L. M., Mouikis, C. G., Dumlop, M. W., Klecker, B., & Sauvaud, J.-A. (2010). A case study of EMIC wave-associated He^+ energization in the outer magnetosphere: Cluster and Double Star 1 observations. Journal of Geophysical Research, 115, A06212. https:// doi.org/10.1029/2009JA014784.

Accepted Article

© 2019 American Geophysical Union. All rights reserved.

Table 1. Proton components used to model the proton distributions observed at about 01:23:14 UT, when *N*e is 550 cm^{-3} and B_t is 263 nT.

Components	n (cm^{-3})	$T_{//}$ (eV)	$T_{\perp}$ (eV)
1	48.00	1	1
2	0.35	7	7
3	0.70	700	350
4	2.00	15×10^3	25×10^3

Table 2. The same to Table 1 but at about 01:20:13 UT, when N_e is 150 cm^{-3} and B_t 230 nT.

Components	n (cm^{-3})	$T_{//}$ (eV)	$T_{\perp}$ (eV)
1	2.30	3	1
2	3.10	24	11
3	4.90	13.3	7.7
4	2.00	70	50
5	0.35	2.0×10^3	1.5×10^3
6	2.0	15×10^3	25×10^3

Accepted Article

© 2019 American Geophysical Union. All rights reserved.

Accepted Article

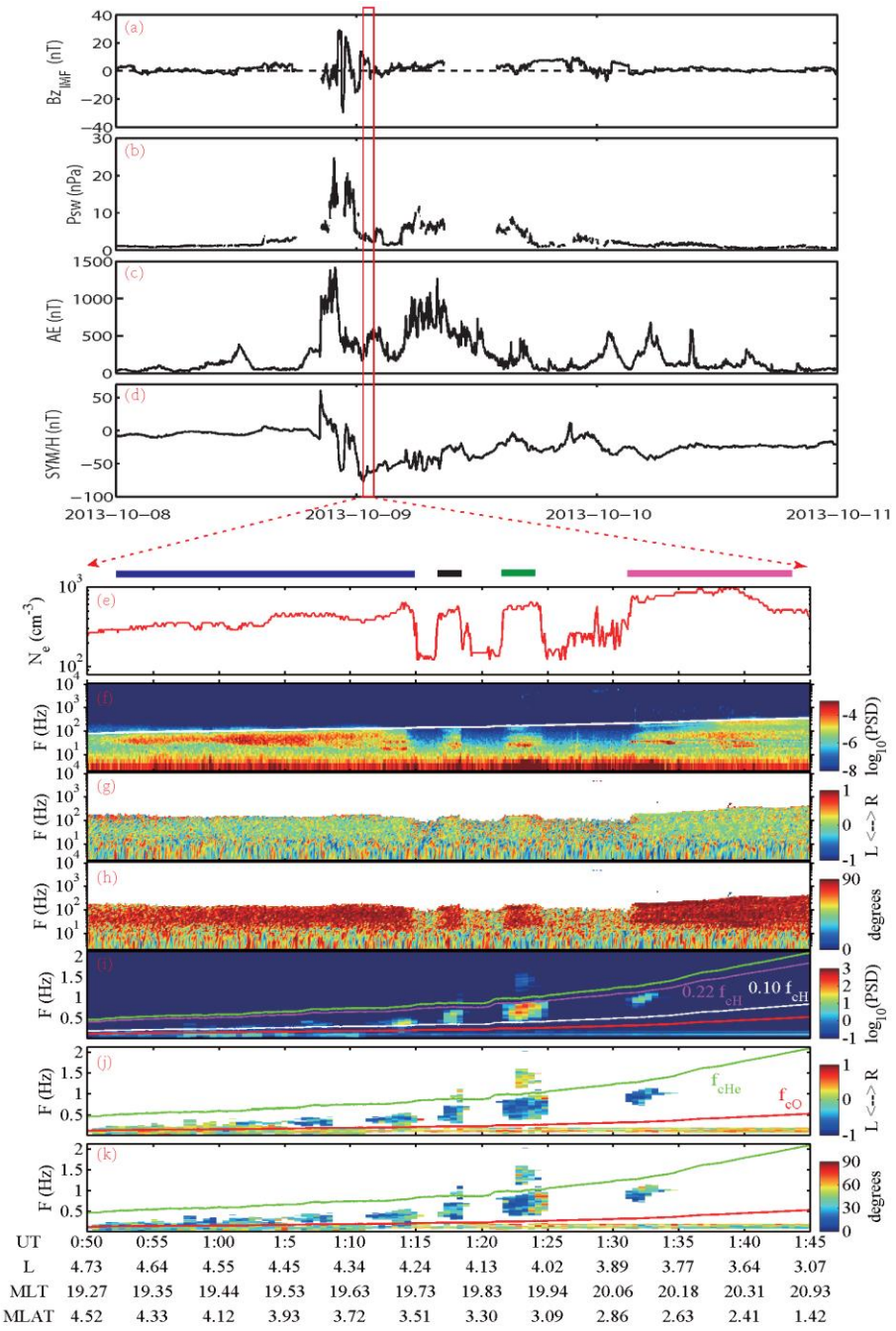

Figure 1. Overview of simultaneously trapping event of EMIC and MS waves. (a-d) B_z component of the interplanetary magnetic field, solar wind dynamic pressures, AE index, and SYM-H index during 8 October 2013 and 10 October 2013. (e) Background plasma densities (N_e). (f-h) Magnetic spectral intensity, ellipticity, and wave normal angles of MS waves. (i-k) Magnetic spectral intensity, ellipticity, and wave normal angles of EMIC waves. The white curve in panel (f) denotes the lower hybrid resonant frequencies, while the green and red curves in panel (i)-(k) denote helium and oxygen ion gyrofrequencies, respectively, and the purple and white curves in panel (i) denote 0.22 f_{cH} and 0.10 f_{cH} (where f_{cH} is proton gyrofrequencies), respectively.

© 2019 American Geophysical Union. All rights reserved.

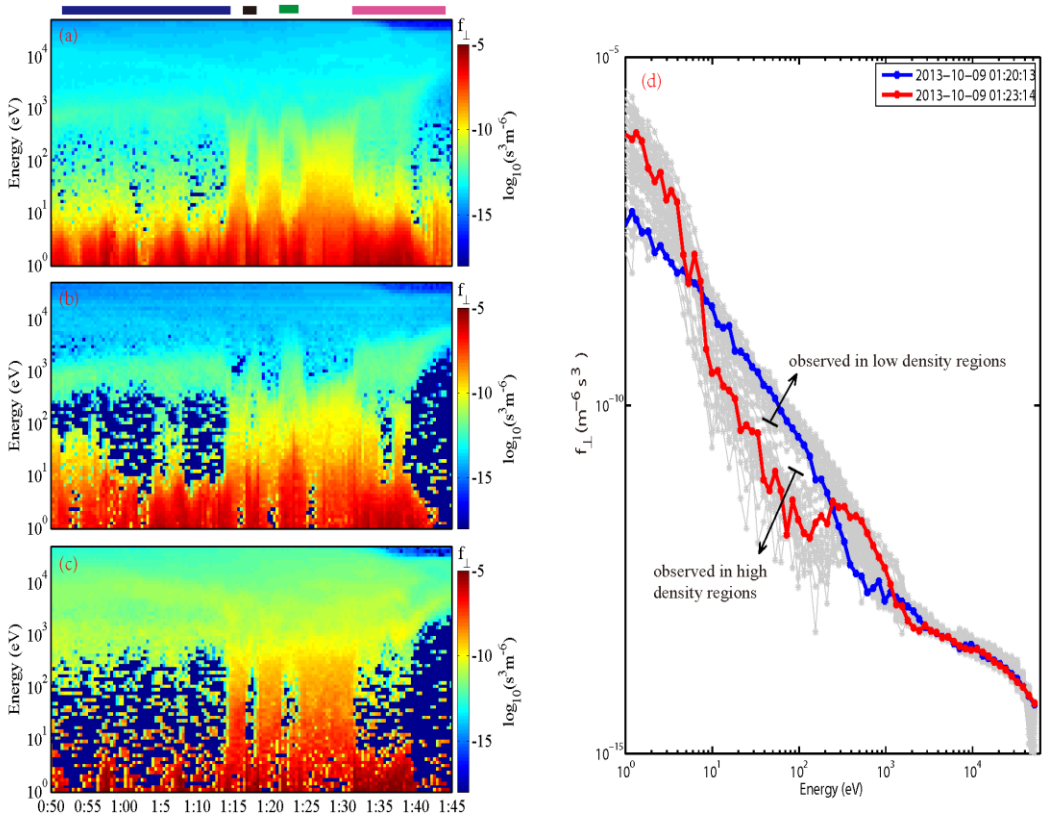

Figure 2. Observed ion velocity distributions between 0050 UT and 0145 UT. (a-c) perpendicular velocity distributions for protons, helium ions, and oxygen ions, respectively. (d) Proton distributions observed between about 0114 UT and 0134 UT (grey curves), observed at about 0120 UT (blue curve), and observed at about 0123 UT (red curve).

Accepted

© 2019 American Geophysical Union. All rights reserved.

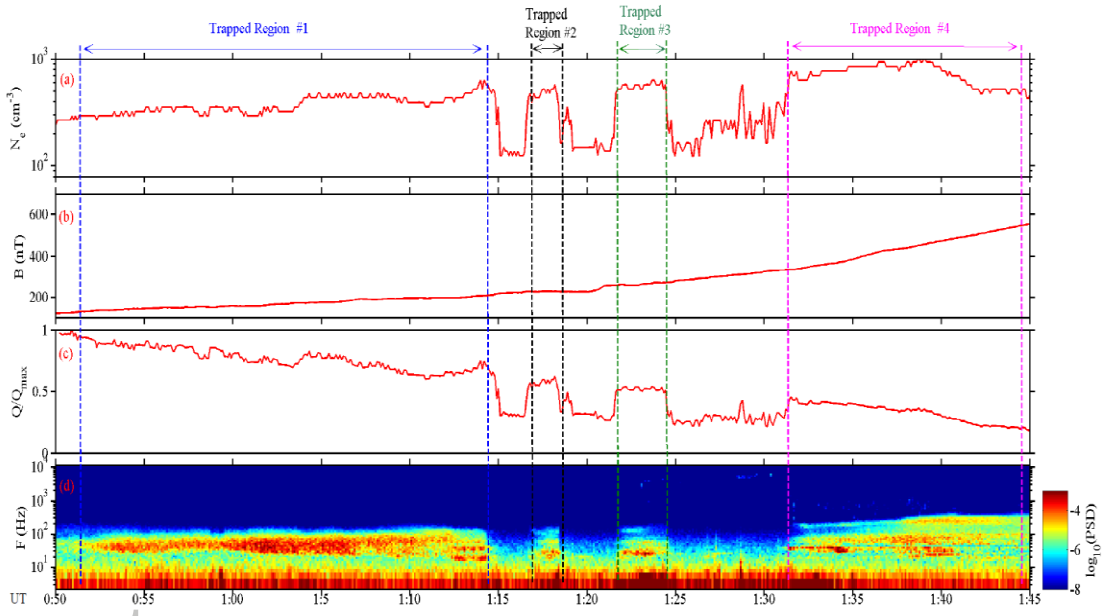

Figure 3. Trapping analysis of MS waves between 0050 UT and 0145 UT. **(a)** Background plasma densities. **(b)** Magnetic field intensity (*B*). **(c)** Calculated Q normalized to its maximum value Q_{max}. **(d)** Magnetic spectral intensity of MS waves.

Accepted Article

© 2019 American Geophysical Union. All rights reserved.

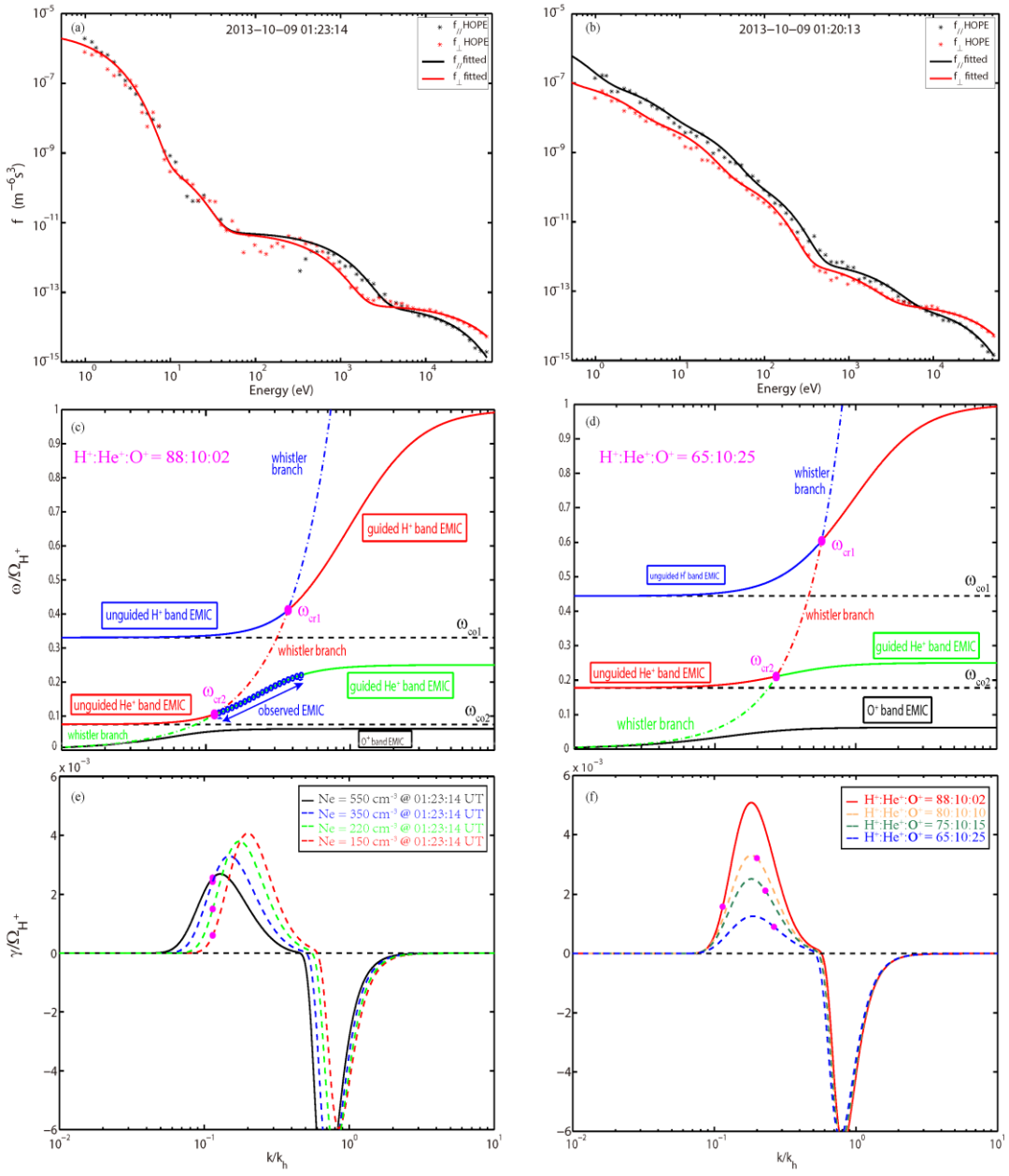

Figure 4. (a–b) Measured (asterisks) and fitted (curves) proton distributions at 01:23:14 UT and 01:20:13 UT, respectively. Red asterisks and curves denote the parallel components, while black ones denote the perpendicular components. **(c–d)** Dispersion relation for ion compositions of H^+:He^+:O^+ = 88:10:2 and 65:10:25, respectively. Purple dots denote the cross-over frequencies (ω_{cr1} and ω_{cr2}), while the dashed horizontal lines denote the cut-off frequencies (ω_{co1} and ω_{co2}). Note that the frequency interval of the observed EMIC waves is marked by blue circles in panel (c). **(e)** Linear growth rate for He^+ band EMIC waves for different plasma densities. (f) Linear growth rate for He^+ band EMIC waves in plasmas with different ion compositions.

© 2019 American Geophysical Union. All rights reserved.

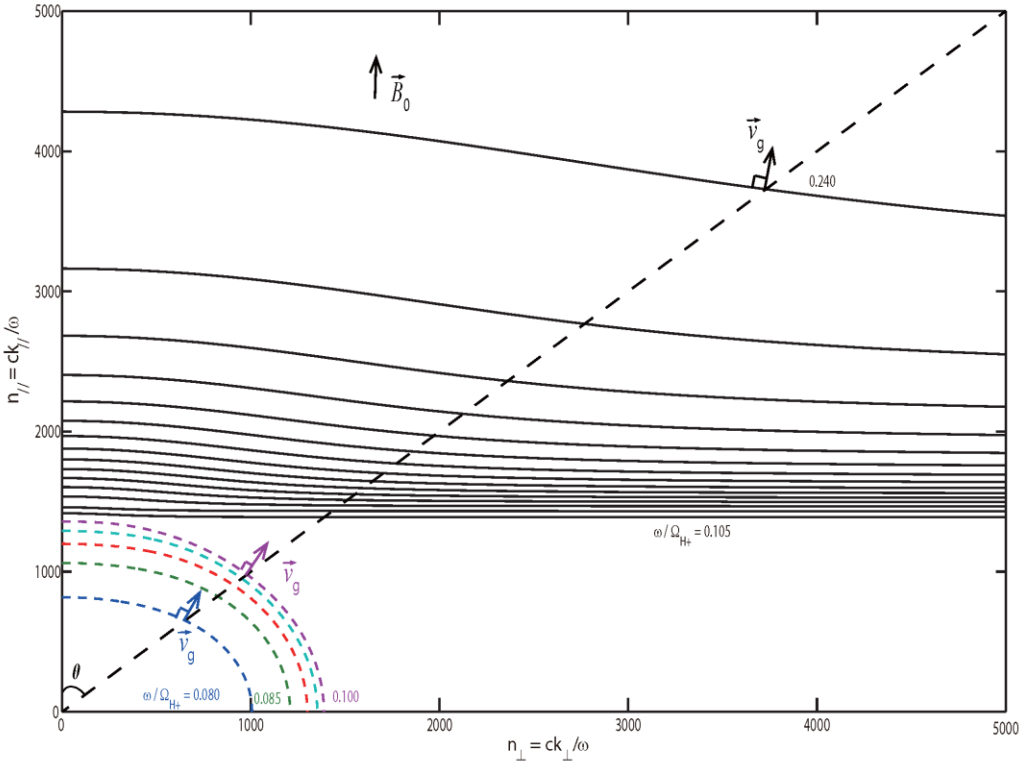

Figure 5. Refractive index surfaces for He^+ band EMIC waves. Guided EMIC waves are shown as solid black curves, while unguided EMIC waves are dashed colored curves.

Accepted

© 2019 American Geophysical Union. All rights reserved.